technical transactions

No. 2021/024

mechanics

sciendo

Depth control for biomimetic and hybrid unmanned underwater vehicles

Marcin Morawski

marcin.morawski@pk.edu.pl | https://orcid.org/0000-0002-7078-2795

Tomasz Talarczyk

tomasz.talarczyk1@gmail.com

Marcin Malec

marcin.malec@pk.edu.pl | https://orcid.org/0000-0001-5232-7425

Chair of Production Engineering, Faculty of Mechanical Engineering, Cracow University of Technology

Scientific Editor: Stanisław Młynarski, Cracow University of Technology
Technical Editor: Aleksandra Urzędowska, Cracow University of Technology Press
Language Verification: Timothy Churcher, Merlin Language Services
Typesetting: Anna Basista, Cracow University of Technology Press

Received: July 7, 2021
Accepted: December 17, 2021

Data Availability Statement: All relevant data are within the paper and its Supporting Information files.

Competing interests: The authors have declared that no competing interests exist.

Citation: Morawski, M., Talarczyk, T., Malec, M., (2021). Depth control for biomimetic and hybrid unmanned underwater vehicles. *Technical Transactions*: *e2021024*. https://doi.org/10.37705/TechTrans/e2021024

Abstract

Unmanned underwater vehicles which use biomimetic mechanisms are becoming increasingly useful in the realisation of tasks requiring silent and efficient propulsion. Complex fish kinematics are simplified to some extent and implemented in such vehicles. One of the essential fish behaviours is their ability to adjust their buoyancy using a swim bladder. This paper covers the issues concerning the implementation of artificial swim bladders as well as depth regulators in two underwater vehicles: biomimetic and hybrid. The control of vehicle depth through buoyancy change was examined in the computer simulation and in the experiment. Two types of artificial swim bladder were tested – a rigid cylinder with a piston and an elastic container with a water pump.

Keywords: BUUV, HUUV, depth control, artificial swim bladder

1. Introduction

Most small and medium-sized standard screw-propelled unmanned underwater vehicles (UUV), both autonomous (AUV) and remotely operated (ROV), utilise their neutral or slightly positive buoyancy in cooperation with vertical thrusters and control surfaces to maintain their depth of operation. In case of ROVs, the proper control of the magnitude of vertical thrust to maintain the desired depth relies on the vehicle's operator, but in some cases, an automatic depth controller may be used for this purpose (Mai et al., 2017). Most of the time, simple sliding mode control or proportional derivative (PD) algorithms are used to control the rpm of vertical thrusters based on the desired depth and actual depth measured mostly by absolute pressure sensors (Maalouf et al., 2015). AUVs, on the other hand, must rely entirely on their autonomously operated on-board control systems in which the depth controller is implemented. As the majority of the motion of the AUV is performed in the direction of the longitudinal axis of the hull, the obvious method for depth control is to adjust the angles of attack of the vehicle's control surfaces (elevators) while the vehicle is moving at a certain speed by means of its main thrusters (Yao et al., 2017). Using additional vertical thrusters for the depth control of AUVs is less common but also possible (Melo & Matos, 2015). In some cases, depth control may be substituted with the control of the distance to the seabed, especially in the case of bed mapping using multibeam echosounders or side scan sonar (Robert et al., 2017), seabed filming (Singh et al., 2014) or subsea cable tracking (Xiang et al., 2016). In these cases, instead of actual depth as an input signal for the depth controller, the actual distance to the seabed is provided by an altimeter. The methods mentioned above are widely and effectively used in various underwater tasks. Their main advantages are their simplicity, reliability, ease of implementation and fast action. As major drawbacks, one could mention the high level of generated noise and the high water turbulence which affects water clarity and reduces the quality of registered video images. These disadvantages are common for screw-propelled underwater vehicles, thus new types of biomimetic underwater vehicles (BUUV) propelled by so-called undulating propellers, which do not have these flaws, are becoming increasingly popular. BUUVs are designed in such a manner as to be able to mimic the visual appearance, dimensions, and kinematics of a real aquatic animals (most commonly fish) or at least some of the features of a selected species. It is obvious that no screw propellers are appropriate in these kinds of vehicles; motion is instead achieved only by properly designed fins in cooperation with mechanisms for generating undulation. Many types of BUUVs can be found in the literature, but only a fraction of them are able to swim freely in a real underwater environment (Anderson & Chhabra, 2006)(Liang et al., 2009)(Low, 2011) and these must be equipped with some sort of depth control subsystems. It remains the case that the majority of BUUVs are prototypes used for laboratory research on fish--like motion (Anton & Listak, 2011)(Lauder, 2015)(Wen et al., 2012) and its application in aquatic vessels (Chu et al., 2012)(Morawski et al., 2014)(Q. S. Nguyen et al., 2011) (Tangorra et al., 2011). This paper covers the problem of designing and implementing a depth control subsystem for free swimming BUUV, which can be used for various underwater inspection tasks. Major steps of the development process of the BUUV were described in the authors' previous work (Morawski et al., 2018). The same depth control methods can be implemented in any kind of underwater vehicle. In some cases, vehicles in which combined screw propellers and undulating propulsion are used – so-called hybrid vehicles (HUUV) – may be desirable to fulfil specific underwater missions (Conry et al., 2013)(Ai et al., 2018)(Cai et al., 2020).

2. Static and dynamic depth control

Using thrusters and vehicle's control surfaces (rudders, elevators) for obtaining the desired depth can be collectively named dynamic depth control methods because they require use of the vehicle's main drive (or drives) to achieve the required speed. Static depth control methods, on the other hand, utilise changes to the vehicle's buoyancy and can be performed without participation of the vehicle's main drive. As far as BUUVs are

https://doi.org/10.37705/TechTrans/e2021024

concerned, dynamic depth control requires the generation of oscillations or undulations of the main drive (tail and caudal fin) in cooperation with changing the angle of attack of the pectoral fins. Sometimes, shifting the centre of gravity (COG) towards the fore part of the vehicle is desired. The effectiveness of this kind of motion is better if the vehicle buoyancy is as close to neutral as possible. In his work, Colquhoun (Colquhoun, n.d.) presented the prototype of a remotely operated robotic fish with a COG shifting mechanism which affects the vehicle's pitch angle. The main thrust was generated by the tail and the caudal fin and at pitch angles of around 21 degrees and a diving rate of 0.07 m/s was achieved. The author also calculated the Froude efficiency for undulating propulsion, which had its peak of 47% at the tail oscillation frequency of 0.9 Hz. The Strouhal number was also calculated to be 1.35 at 0.9 Hz. Depth control using a PID algorithm for adjusting the angle of attack of the pectoral fins of a small free-swimming fish robot was studied by Morgansen, Triplett and Klein (Morgansen et al., 2007) both in simulations and in experimental research. The depth control was tested in two conditions: when the robot was propelled by an undulating tail with a caudal fin and when the robot was propelled by oscillating pectoral fins. The maximum depth error achieved in the experiment was ±10 cm. Dynamic depth control of miniature robotic fish using pectoral fins and a fuzzy PD controller was also studied by Zhang et. al. (Le Zhang et al., 2007). The robot needed to swim forward at a certain speed to be able to reach the desired depth. The depth controller input was not the depth error, as one could expect, but rather the vehicle's trim needed to achieve the set depth. The fuzzy controller utilised triangular membership functions for input and output signals evenly distributed across their normalised domains. The actual vehicle's depth was measured by an on-board pressure sensor while its orientation in water was measured by a video camera suspended above the laboratory tank. Thus, the vehicle's control system relied on external sensors and cannot be used for a free swimming robot. A similar fuzzy depth controller was used by Niu et. al. (Niu et al., 2012) but for a different type of biomimetic underwater vehicle mimicking the cownose ray (la. *Rhinoptera bonasus*). In this case, the input signals for the depth controller were the depth error and its rate of change measured indirectly by the hydrostatic pressure sensor. The output signal from the depth controller was the angle of attack of elevators located on each side of the vehicle's stern. The main thrust was generated by two oscillating pectoral fins. The diving rate achieved during the experimental research was around 0.35 m/s at 25 degrees of tail's elevator inclination. This robotic ray was able to swim freely and was remotely operated from shore via a 433 MHz FM radio link. A slightly different approach was taken by Yu et. al. (Yu et al., 2016) for the simultaneous depth and direction control of robotic fish, the task of which was to navigate underwater towards a submerged artificial landmark. The position of the landmark was identified by the robot's vision system and on-board camcorder. The vehicle's main thrust was generated by the tail and caudal fin, whereas the depth was changed by adjusting the angle of attack of the pectoral fins. The fuzzy sliding mode controller was used for depth control and it worked quite well. In the executed experiment, the mean depth error was 1.56 cm with a variance of 7.38 cm^2.

Most of small-sized biomimetic underwater vehicles described in the literature use dynamic depth control (or no depth control at all) by means of pectoral fins. Rarely is the vehicle's COG shifting mechanism or buoyancy change used in addition to pectoral fins in depth control systems. Nguyen et. al. (Minh-Thuan et al., 2011)(T.-T. Nguyen et al., 2011) implemented a tiny ballast tank as an artificial swim bladder for their physical model of Pearl Arowana (la. *Scleropages jardini*). This tank is located in the fore part of the vehicle's hull and thus also changes the position of the robot's COG when filled with water. This artificial swim bladder was in the form of a cylinder directly connected to the front wall of the hull. A piston, driven by a screw-nut mechanism and a small servomotor, is placed inside the cylinder. The capacity of the cylinder is 12 ml, which is 9.6% of the vehicle's volume. Other experimental research (Minh-Thuan et al., 2011) present results of robot diving rates for different amounts of water in the ballast tank (different piston positions) as well as different additional weights attached to the vehicle's hull (increased negative buoyancy) although no depth controller was described. Buoyancy tanks of a similar design were

implemented in a small free-swimming robotic fish with a soft tail described by Katzschmann et al. (Katzschmann et al., 2018). These tanks are in the form of small cylinders with pistons driven by miniature linear actuators. The vehicle is equipped with two such artificial swim bladders located symmetrically on each side of the robot's centre of gravity – one in the fore and one in the aft part of the hull. Equal changes of their volume do not affect the vehicle's trim. The robot was remotely operated by the diver using a watertight control unit and custom made acoustic modems. The desired depth is then set manually by the diver and PID algorithm implemented in the robot's on-board control system is responsible for maintaining this depth. Furthermore, the angles of attack of the robot's pectoral fins are adjusted during depth change. An interesting concept of an underwater crawling robot capable of changing its buoyancy between positive and negative was described by Hangil and Son-Cheol (Joe & Yu, 2016). Having six legs, the robot is able to crawl upside down underneath an ice layer on the water surface, measuring its thickness using a laser or ultrasound ranging system. In this case, the robot is positively buoyant. When obstacles on the robot's path need to be avoided, the vehicle's buoyancy was changed to neutral or slightly negative, which helps the vehicle to perform a type of inverse jump over the obstacle. The buoyancy is then changed back to positive and the robot "sticks" to the ice upside down. The robot is controlled remotely using a tether and when its task is completed, the buoyancy is changed to highly negative and the vehicle is pulled by the tether up to the surface and dragged out of the water through the same hole in the ice from which it was launched. A simple tank filled with water by a miniature reversible pump is used to adjust the robot's buoyancy. No depth controller is used. A different approach to the buoyancy change systems was described in other work (Aras et al., 2015). A flexible tank was used with a bidirectional pump to control the water flow. The main two tasks of the flexible tank were to maintain depth with less power consumption than the propulsion-based depth control system and enable the ROV to move deeper when the thrusters reach the maximal vertical thrust. A depth regulator was proposed to achieve static depth control, but no final results of controlling the AUV depth were presented. Different methods of combining a propulsion system and a variable buoyancy system for the depth control of an AUV have been presented (Medvedev et al., 2017b). The main goal of this research was to increase the cruising range of the vehicle by reducing the energy consumption of the depth control system. Four different methods for minimising the response time and energy consumption were tested.

3. Static depth control subsystems in the BUUV and HUUV

The biomimetic unmanned underwater vehicle presented in Figure 1 was designed and constructed during a Polish national research project which was aimed at the development of vehicles with silent propulsion, capable of performing various underwater inspection tasks. New types of biomimetic propellers with elastic fins and specially designed drive mechanisms were used instead of screw propellers to reduce the noise generated by the vehicle's propulsion subsystem. The robot is equipped with a tail section comprised of two rigid segments connected in series with an elastic caudal fin attached to the end of the second segment. The tail is responsible for generating the vehicle's main thrust by means of the proper synchronisation of oscillations of its segments which results in the undulation of the tail and caudal fin. Additional thrust can also be generated by two independently driven oscillating pectoral fins, with rigid front sections and flexible end sections. The BUUV and its subsystems, as well as the design process, are described in the authors' previous work (Morawski et al., 2018). Views and dimensions of the vehicle are presented in Figure 1. The mass of the vehicle is 64 kg and its buoyancy is close to neutral. The vehicle was designed to operate at depths of up to 30 m.

When the vehicle is in motion, the depth can be controlled either by adjusting the angle of attack of both pectoral fins (dynamic depth regulation), or by means of

https://doi.org/10.37705/TechTrans/e2021024

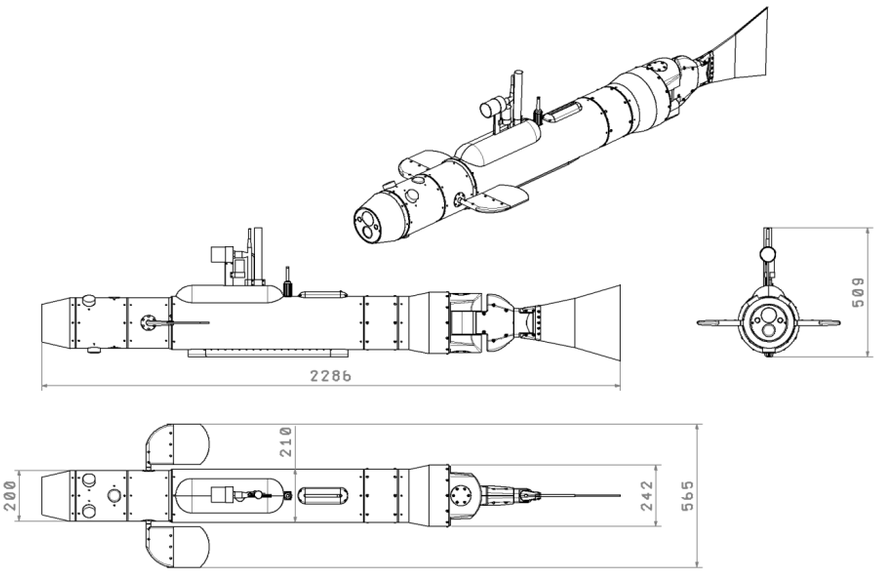

Fig. 1. Views and dimensions of the BUUV

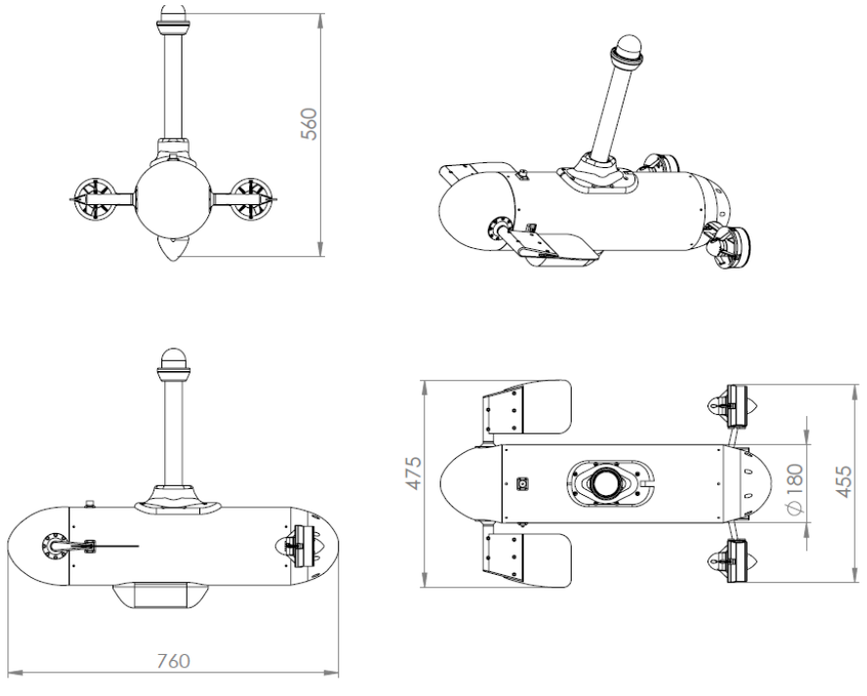

Fig. 2. Views and dimensions of the HUUV

the internal ballast tank (static depth regulation). Dynamic depth regulation of the BUV is not within the scope of this paper. In the BUUV presented in Figure 1, the internal ballast tank is in the form of a cylinder with a piston driven by a lead screw and a servomotor with position feedback. Thus, the precise positioning of the piston inside the cylinder is possible. This gives the control system information about the amount of water inside the cylinder. Vehicle buoyancy can then be calculated accordingly. The piston position is controlled by the signal from the PID depth controller. The actual depth of the vehicle is measured indirectly by the hydrostatic pressure sensor.

The hybrid unmanned underwater vehicle presented in Figure 2 was designed and constructed to combine the advantages of two types of propulsion systems: fast, loud, and energy--consuming screw propellers; quiet, efficient but slow undulating pectoral fins. The mass of the vehicle is 18.6 kg and the buoyancy is positive at around 0.6 kg due to the large mast. Therefore, the variable buoyancy system (VBS) was used to allow regulation of the static depth of the vehicle. The second reason for using VBS is to support the biomimetic propellers in submersion. Due to the low dynamic and low generated thrust of the silent propulsion system compared to the screw propellers, the change in buoyancy has a significant impact on the change of the vehicle immersion when the mast is above the surface of the water.

The variable buoyancy system of the HUUV consists of 4 parts: the flexible tank which is placed in a rigid container, a bidirectional water gear pump, a hydrostatic pressure sensor to measure the actual depth of the vehicle and the controller with an implemented depth regulator. To prevent rupture of the flexible tank, a rigid container was used with two additional pressure sensors. One sensor was used to measure pressure inside the vehicle's hull and the other was used to measure pressure inside the flexible tank. These two additional sensors are not involved directly in depth regulation but are used in emergency conditions.

4. Simulation and experimental research

Vertical motion of the vehicle during static depth regulation can be derived from Fossen's equations (Fossen, 2011) of 6 DOF underwater vehicle motion, and can be described with the following formula (1):

$$(m+m_w)\ddot{z} = P-(D_L+D_{NL})\dot{z}-B(t,z)+Z_k \tag{1}$$

where:

- z – vertical coordinate (depth of the vehicle) with 0 value on the surface of the water,
- m – mass of the vehicle,
- m_W – added mass dependent on the vehicle motion along the vertical axis,
- D_L – first-order (linear) damping coefficient along the vertical axis of motion,
- D_{NL} – second-order (nonlinear) damping coefficient along the vertical axis of motion,
- P – weight of the vehicle calculated on the basis of $m \cdot g$,
- g – gravity acceleration,
- $B(t,z)$ – buoyancy force as a function of time and vertical coordinate z,
- z_k – other external forces acting on the vehicle (disturbances).

Damping coefficients in the above equation (1) were in this case replaced by the well-known formula below (2) in which: $C_d(Rn)$ is the drag coefficient dependent on Reynolds number, ρ is water density and A is the area of the vehicle's cross section perpendicular to the direction of motion. It is assumed that the hydrodynamic damping is mainly caused by vortex shedding behind the vehicle's hull moving along the z axis.

$$(DL+D_{NL}) = \frac{c_d(Rn)\rho A}{2}\dot{z} \tag{2}$$

The buoyancy force acting on the vehicle can be expressed by the function below (3), where the vehicle's submerged volume is $V_p(t, z)$ and the volume of water inside the ballast tank is $V_b(t)$.

$$B(t,z) = \gamma(V_p(t,z)-V_b(t)) \tag{3}$$

By rearranging equation no. 1 and taking into account equations 2 and 3, acceleration of the vehicle during vertical motion is given by the equation below (4).

$$\ddot{z} = \frac{mg-0.5C_d\rho A\dot{z}^2-\gamma V_p(t,z)-\gamma V_b(t)+Z_k)}{(m+m_{\dot{W}})} \tag{4}$$

The vehicle's submerged volume depends on time (t) and vertical coordinate (z), whereas the volume of water inside the ballast tank depends on the depth control system and also changes over time (t). In equation no. 2, γ is the water specific weight, which is the product of water density and gravitational acceleration.

Having the precise CAD models of the vehicles, $V_p(t, z)$ was numerically approximated with the piecewise function below (5) using the least squares method.

$$V_p(t,z) = \begin{cases} V_p \text{ for } z \geq z_0 \\ f_1(z) \text{ for } z_0 > z \geq z_1 \\ f_2(z) \text{ for } z_1 > z \geq z_2 \end{cases} \tag{5}$$

where:

- V_p – the volume of the totally submerged vehicle,
- $f_1(z)$ and $f_2(z)$ – functions describing the submerged part of the vehicles while the other parts of the vehicle (mast and antennas) are above the surface of the water,
- z_0, z_1, z_2 – values along the vertical coordinate axis at which specific parts of the vehicle are starting to emerge above the water surface (those values depend on the geometry of the vehicle and can be obtained from its CAD model).

https://doi.org/10.37705/TechTrans/e2021024

For the BUUV, the obtained values of: V_p, $f_1(z)$, $f_2(z)$, z_0, z_1, z_2, are as follows:
$V_p = 0.064027$ m^3
$f_1(z) = -0.0025\,z^2 + 0.0023\,z + 0.0641$:
($R^2 = 0.96$)
$f_2(z) = 1234.90\,z^5 + 1904.30\,z^4 + 1159.30\,z^3 + 346.62\,z^2 + 50.88\,z + 3.00$:
($R^2 = 1$)
$z_0 = 0$ m
$z_1 = -0.22$ m
$z_2 = -0.4$ m

In the above case, z is measured from the water surface to the uppermost part of the BUUV. The vehicle is totally submerged at $z_0 = 0$ m and the piston is located in the middle of the ballast tank. Shifting the piston one way in the ballast tank causes the vehicle to submerge further. The total submerged volume is in this case 0.064027 m^3. When the piston is shifted the other way, the vehicle's mast with camera and antennas begin to emerge above the water surface, decreasing the remaining submerged volume. Negative values of z are above the water surface. The BUUV is capable of statically surfacing as far as $z = -0.25$ m. Further approximation of the submerged volume is only for the sake of dynamic motion.

For the HUUV, the obtained values of: V_p, $f_1(z)$, $f_2(z)$, z_0, z_1, z_2, are as follows:
$V_p = 0.019310$ m^3
$f_1(z) = -18.234\,z^6 - 17.432\,z^5 - 6.2715\,z^4 - 1.0232\,z^3 - 0.0666\,z^2 + 0.0013\,z + 0.0193$:
($R^2 = 0.96$)
$f_2(z) = 7.9916\,z^3 + 7.7547\,z^2 + 2.5086\,z + 0.2893$:
($R^2 = 1$)
$z_0 = 0$ m
$z_1 = -0.3$ m
$z_2 = -0.4$ m

In the case of HUUV, z is measured from the surface of the water to the uppermost part of the HUUV. The HUUV is totally submerged at $z_0 = 0$ m with the ballast tank entirely filled with water. The total submerged volume in this case is 0.019310 m^3. When the ballast tank is empty, the vehicle's mast with camera and antennas is above the surface of the water. The HUUV is only capable to statically surfacing as far as $z = -0.3$ m. Further approximation of the submerged volume is only for the sake of dynamic motion.

Static depth regulation depends on changes in the vehicle's buoyancy resulting from changing the amount of water inside the ballast tank ($V_b(t)$). In the BUUV, this tank is in the form of a cylinder with a piston driven by a servomotor with an additional gearhead and a lead screw, thus the $V_b(t)$ can be expressed with the formula below (6). The maximum volume of the cylinder is 0.6 dm^3.

$$V_b(t)_{BUUV} = \frac{(\alpha d^2 ip)}{8} \tag{6}$$

where:

- α – angle of rotation of the servomotor's shaft (controlled by the static depth regulator),
- d – inner diameter of the cylinder,
- i – gear ratio of the additional gearhead,
- p – pitch of the lead screw.

In the HUUV, the ballast tank is in the form of an elastic bladder filled with water by means of the miniature bidirectional gear pump, thus the $V_b(t)$ depends on the pump flow rate and the maximum possible volume of the stretched bladder. The bladder is inserted into the steel frame to prevent its rupture due to excess stretching. This limits its maximum volume to 0.8 dm^3. $V_b(t)$ for the HUUV can be expressed with the formula below (6).

$$V_b(t)_{HUUV} = \int_{V_{\min}}^{V_{\max}} \dot{v}(t)dt \tag{7}$$

where:

$\dot{v}(t)$ – flow rate of the pump (controlled by the static depth regulator, the maximum flowrate is $0.6\frac{\mathrm{dm}^3}{\mathrm{min}}$ in each direction),

$V_{\max}$ – maximum possible volume of the ballast tank,

$V_{\min}$ – small residual amount of water in the ballast tank.

Other parameters of the BUUV and HUUV are presented in Table 1.

Table 1. Main parameters of the BUUV and HUUV

Parameter	BUUV	HUUV
mass (m) [kg]	63.90	18.58
added mass $m_{\dot{W}}$ [kg]	12.77	6.5
horizontal cross section area (A) [m²]	0.45231	0.18251
drag coefficient in vertical motion C_d	0.71	0.78
maximal submerging speed $\dot{z}_{\max}$ [m/s]	0.06	0.225
maximal emerging speed $\dot{z}_{\max 2}$ [m/s]	−0.07	−0.09
maximal volume of the ballast tank (V_b) [m³]*f* the ballast tank e table 1.ntone.ng to emerge above woater surfece	0.0006	0.0008
ratio of the ballast tank volume to vehicle submerged volume	0.009	0.042

For both BUUV and HUUV, the mathematical models of static depth regulation (vertical motion underwater) were implemented in the SciLab/Xcos software in order to tune the PID controller parameters. Both vehicles have hulls of similar shape and differ mainly in their length, mass, mass distribution, hull volume, and horizontal cross section area. Both models varied in terms of implementation of the VBS. In the case of the BUUV, the volume of water inside the ballast tank was calculated in simulation based on the piston position (dependent on the angle of rotation of the servomotor shaft), whereas in the case of the HUUV, the volume of water inside the ballast tank had to be integrated on the basis of the actual water-pump flow rate. Thus, the output signal from the static depth controller of the BUUV was the angle of rotation of the servomotor shaft and consequently, the piston position inside the ballast tank. The output signal from the static depth controller of the HUUV was the pump flow rate. In both cases, the input signals for the static depth controller were depth errors. The water pump flow rate integration in the case of the HUUV was done only in the simulation, thus no error accumulation over time occurred. In the real HUUV, this integration is done mechanically by the pump-tank system. The

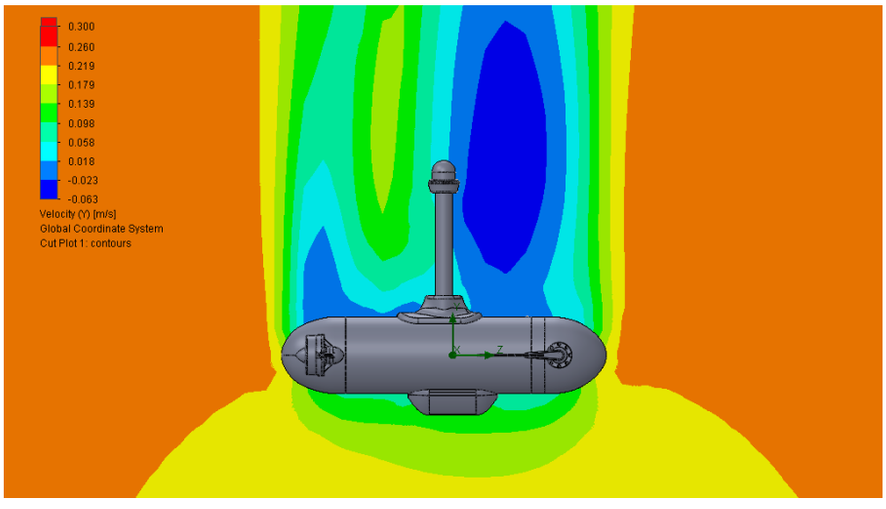

Fig. 3. Velocity map from CFD analysis of vertical flow around the HUVV

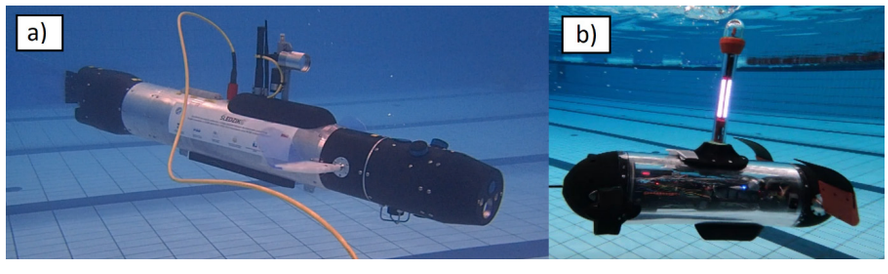

Fig. 4. Vehicles in the swimming pool a) BUUV, b) HUUV

https://doi.org/10.37705/TechTrans/e2021024

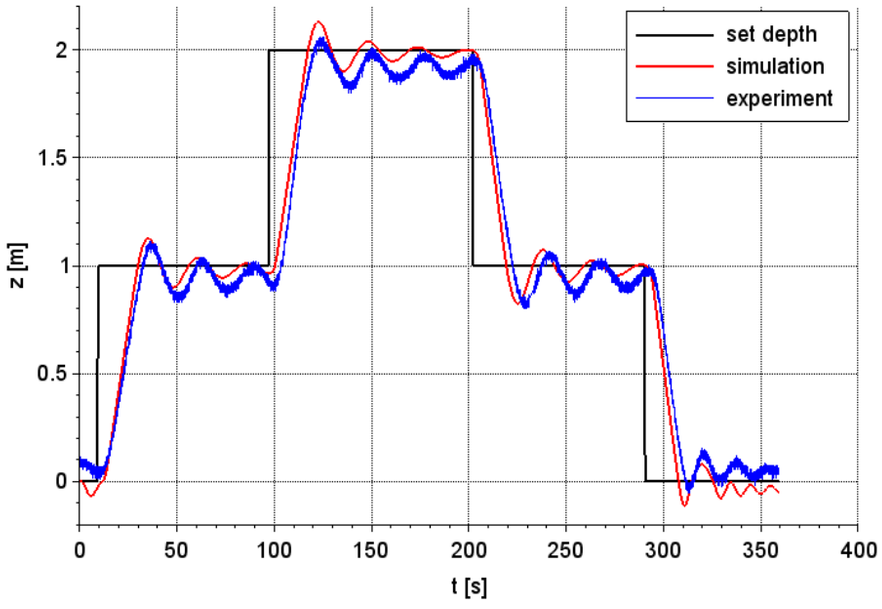

Fig. 5. Static depth regulation for the BUUV

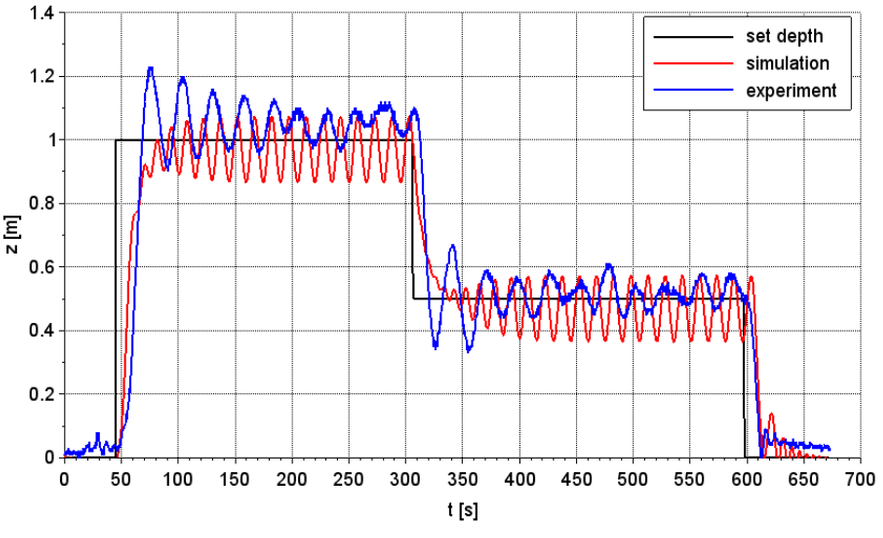

Fig. 6. Static depth regulation for the HUUV

control system of the real HUUV does not calculate the volume of water inside the ballast tank – this is not necessary. The BUUV and HUUV have cylindrical hulls of the same diameter (0.2 m). C_d coefficients for the BUUV and HUUV were obtained from the CFD analysis of the vehicle hulls in a steady flow (Fig. 3) in the Solidworks® Flow Simulation software. The model was then tested to check if the same maximal submerging speed as measured in the experiment in static water is obtained with an entirely filled ballast tank (minimum buoyancy of the vehicle). Added mass $M_{\dot{W}}$ was estimated based on the force and drag coefficient calculated using the CFD analysis and the method described in the literature (Morawski et al., 2020). Static depth regulator parameters were tuned in the simulation. For the BUUV, the PD controller gave satisfactory results (fast response time and small overshoot). For the HUUV, a slight modification of the classic PD controller was necessary. Instead of the derivative of depth error, the vehicle speed was multiplied by the negative value of the derivative gain. This reduced the vertical speed of the vehicle near the set value of depth and reduced the amplitude of oscillations around the set depth value. A similar approach can be found in the literature (Medvedev et al., 2017a). In the simulation, it was assumed that there were no external disturbances (Z_k = 0) in order to be able to compare the results with the results of the experiment performed in still water in the swimming pool.

Depth regulation for both vehicles was also tested in still water in the swimming pool (Fig. 4). The results for the BUUV and HUUV are presented in Figures 5 and 6, respectively.

5. Discussion

In the BUUV, the static depth regulator was tuned as PD with a proportional gain of k_P = 0.25 and a derivative gain of k_D = 0.15. The response of the regulator for a given set depth signal measured in the experiment corresponds to the results of the simulation, proving that the proposed model is correct and can be used to tune static depth regulators for systems utilising piston-based VBS. In this case, a small overshot is present (around 10%), but this is acceptable. Depth oscillations are suppressed quite quickly. The steady state depth error may be present if the vehicle is not properly ballast to achieve as close to neutral buoyancy as possible with the piston of the VBS located in the middle of the cylinder. This assures the

same change in the BUUV's buoyancy in the up and down directions of vertical motion underwater. The rise time of the depth signal (t_r = 11 s) mainly depends on the maximal speed of the BUUV in the *z* axis, which is the consequence of the ratio of the ballast tank volume to the vehicle's submerged volume and thus the maximal change in vehicle buoyancy.

VBS in the HUUV is different than in the BUUV and the classic PD controller was not working properly which caused a high overshoot in step response as well as depth oscillations of a substantial amplitude. The HUUV buoyancy is changed by pumping water either in or out of the elastic bladder with the miniature gear pump with a fairly small flow rate. This introduces a delay to the system and the static depth regulator needs to slow down the vehicle before the desired depth is reached. In this case, the derivative term in the classic PD controller was replaced by multiplying the vehicle's vertical speed by the negative value of the derivative gain. Thus, the output signal from the controller was a sum of the product of depth error and proportional gain with the product of the vehicle speed and negative derivative gain. In the simulation, k_P = 1 and k_D = 10. In the experiment, k_P and k_D were scaled up to properly calculate the PWM signal for the gear pump. Nevertheless, some oscillations are present in the depth signal. The amplitude of those oscillations depends on the vehicle drag coefficient and the pump flow rate. The maximal amplitude is around 0.1 m, which is an acceptable result.

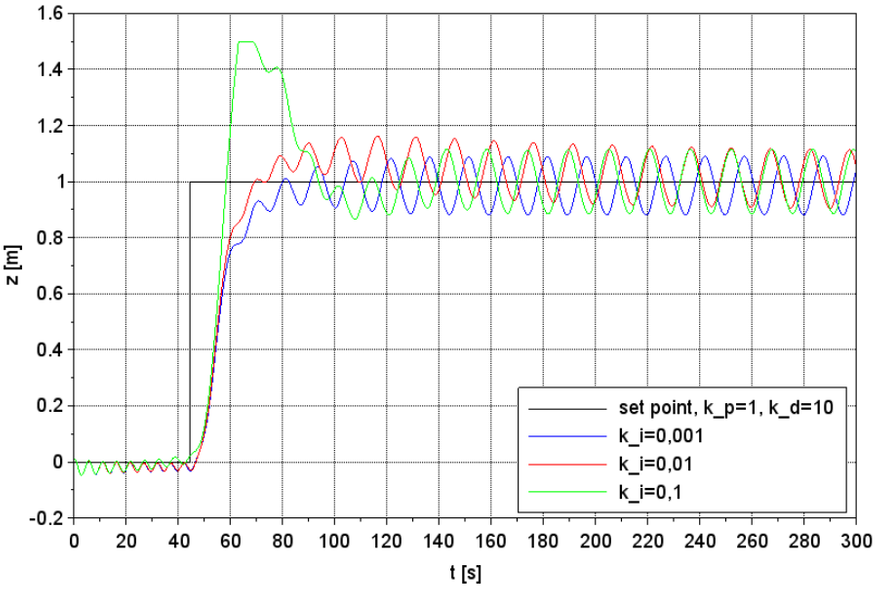

Fig. 7. Influence of the k_I coefficient on the simulated depth regulation for the HUUV

The BUUV as well as the HUUV have rather small ballast tanks in comparison to their total volume. Furthermore, the water flowrate in and out of these ballast tanks is small so the depth regulation systems have a fairly high inertia. In both the BUUV and the HUUV PD controller and the modified PD controller respectively turned out to be sufficient to control the vehicles' depth with an acceptable error. Adding integral term in depth regulators of both vehicles did not improve the quality and stability of depth regulation in the simulation (Fig. 7). A similar effect was observed in the experiment. Depth oscillations shown especially for the HUUV (Fig. 6) could not be dampened further by increasing the derivative term gain due to the mechanical limitations of the real system, especially the small flowrate of the water pump and its dependency on the actual depth (external pressure) as well as the pressure sensor inaccuracy. These limitations was not taken into consideration in the simulation, thus in the simulated conditions, increasing k_D indeed dampens the

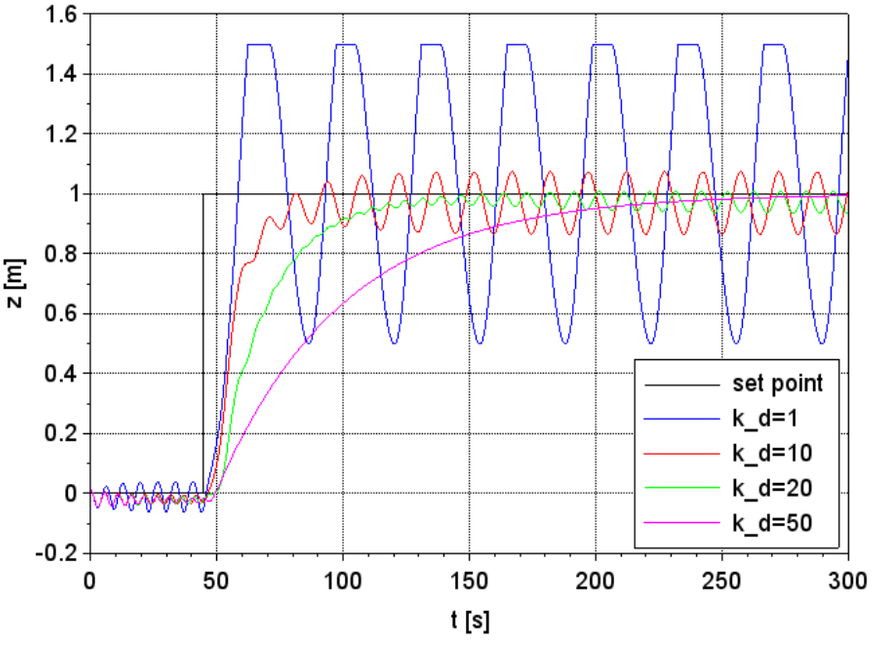

Fig. 8. Influence of the k_D coefficient on the simulated depth regulation for the HUUV

https://doi.org/10.37705/TechTrans/e2021024

step response of the depth regulation (Fig. 8) and increases regulation time. In the simulation, the maximum depth was also limited to 1.5 m as this was the maximal depth of the swimming pool in the experiment.

6. Summary

In this paper, a study of static depth regulators for underwater vehicles with different variable buoyancy systems has been presented. The BUUV and the HUUV were designed and built at the Faculty of Mechanical Engineering of Cracow University of Technology. Both vehicles have a similar hull shape but different masses and lengths, which limits the possibility to install VBS. In the HUUV, the installation of piston-based VBS is virtually impossible due to the limited space inside the hull. The experiment and the simulation both showed that similar static depth regulation as in the BUUV can be achieved using an elastic bladder with a miniature water gear pump to change the vehicle buoyancy. The presented mathematical models as well as their implementation in Scilab/Xcos software proved useful for tuning depth regulators. Larger ballast tanks in both vehicles as well as water pumps with greater flow rate would be desirable to achieve a quicker step response of depth regulation and depth oscillation mitigation. In future work, a study of dynamic depth regulation using adjustable lateral fins as well as its influence on the static depth regulation will be performed for both types of vehicles.

References

Ai, X., Kang, S., & Chou, W. (2018). System Design and Experiment of the Hybrid Underwater Vehicle. *2018 International Conference on Control and Robots*, *ICCR 2018*, 68–72. https://doi.org/10.1109/ICCR.2018.8534493

Anderson, J.M., & Chhabra, N.K. (2006). Maneuvering and Stability Performance of a Robotic Tuna. *Integrative and Comparative Biology*, *42*(1), 118–126. https://doi.org/10.1093/icb/42.1.118

Anton, M., & Listak, M. (2011). Hydrodynamic optimization of a relative link lengths for a biomimetic robotic fish. *2011 15th International Conference on Advanced Robotics (ICAR)*, 530–535. https://doi.org/10.1109/ICAR.2011.6088644

Aras, M.S.M., Abdullah, S.S., Zambri, M.K.M., & Basar M.F. (2015). *Auto depth control for underwater remotely operated vehicles using a flexible ballast tank system*. https://www.researchgate.net/publication/283533128_Auto_depth_control_for_underwater_remotely_operated_vehicles_using_a_flexible_ballast_tank_system

Cai, M., Wang, Y., Wang, S., Wang, R., Ren, Y., & Tan, M. (2020). Grasping Marine Products with Hybrid-Driven Underwater Vehicle-Manipulator System. *IEEE Transactions on Automation Science and Engineering*, *17*(3), 1443–1454. https://doi.org/10.1109/TASE.2019.2957782

Chu, W.-S., Lee, K.-T., Song, S.-H., Han, M.-W., Lee, J.-Y., Kim, H.-S., Kim, M.-S., Park, Y.-J., Cho, K.-J., & Ahn, S.-H. (2012). Review of biomimetic underwater robots using smart actuators. *International Journal of Precision Engineering and Manufacturing*, *13*(7), 1281–1292. https://doi.org/10.1007/s12541-012-0171-7

Colquhoun, C.T. (n.d.). *Development of a biomimetic robotic fish*. Retrieved July 2, 2019, from http://citeseerx.ist.psu.edu/viewdoc/download?doi=10.1.1.538.7314&rep=rep1&type=pdf

Conry, M., Keefe, A., Ober, W., Rufo, M., & Shane, D. (2013). BIOSwimmer: Enabling technology for port security. *2013 IEEE International Conference on Technologies for Homeland Security*, *HST 2013*, 364–368. https://doi.org/10.1109/THS.2013.6699031

Fossen, T.I. (2011). *Handbook of marine craft hydrodynamics and motion control*. Wiley.

Joe, H., & Yu, S.-C. (2016). Iceberg worm: Biomimetic AUV for sea ice thickness survey using non-contact laser ultrasonic method. *2016 IEEE/OES Autonomous Underwater Vehicles (AUV)*, 44–48. https://doi.org/10.1109/AUV.2016.7778718

Katzschmann, R.K., DelPreto, J., MacCurdy, R., & Rus, D. (2018). Exploration of underwater life with an acoustically controlled soft robotic fish. *Science Robotics*, *3*(16), eaar3449. https://doi.org/10.1126/scirobotics.aar3449

Lauder, G.V. (2015). Fish Locomotion: Recent Advances and New Directions. *Annual Review of Marine Science*, *7*(1), 521–545. https://doi.org/10.1146/annurev-marine-010814-015614

Le Zhang, We, Yonghui Hu, Dandan Zhang, & Long Wang. (2007). Development and depth control of biomimetic robotic fish. *2007 IEEE/RSJ International Conference on Intelligent Robots and Systems*, 3560–3565. https://doi.org/10.1109/IROS.2007.4398997

Liang, J., Wei, H., Wang, T., Wen, L., Wang, S., & Liu, M. (2009). Experimental Research on Biorobotic Autonomous Undersea Vehicle. In *Underwater Vehicles*. InTech. https://doi.org/10.5772/6702

Low, K.H. (2011). Current and future trends of biologically inspired underwater vehicles. *2011 Defense Science Research Conference and Expo (DSR)*, 1–8. https://doi.org/10.1109/DSR.2011.6026887

Maalouf, D., Creuze, V., Chemori, A., Tamanaja, I.T., Mercado, E.C., Muñoz, J.T., Lozano, R., & Tempier, O. (2015). Real-Time Experimental Comparison of Two Depth Control Schemes for Underwater Vehicles. *International Journal of Advanced Robotic Systems*, *12*(2), 13. https://doi.org/10.5772/59185

Mai, C., Pedersen, S., Hansen, L., Jepsen, K., & Yang, Z. (2017). Modeling and Control of Industrial ROV's for Semi-Autonomous Subsea Maintenance Services. *IFAC-PapersOnLine*, *50*(1), 13686–13691. https://doi.org/10.1016/J.IFACOL.2017.08.2535

Medvedev, A.V., Kostenko, V.V., & Tolstonogov, A.Y. (2017a). Depth control methods of variable buoyancy AUV. *2017 IEEE OES International Symposium on Underwater Technology*, *UT 2017*. https://doi.org/10.1109/UT.2017.7890333

Medvedev, A.V., Kostenko, V.V., & Tolstonogov, A.Y. (2017b, March 29). Depth control methods of variable buoyancy AUV. *2017 IEEE OES International Symposium on Underwater Technology*, *UT 2017*. https://doi.org/10.1109/UT.2017.7890333

Melo, J., & Matos, A. (2015). A Pitch-Depth Bottom Following Controller for AUVs using Eigenstructure Assignment. *IFAC-PapersOnLine*, *48*(16), 43–48. https://doi.org/10.1016/J.IFACOL.2015.10.256

Minh-Thuan, L., Truong-Thinh, N., & Ngoc-Phuong, N. (2011). Study of artificial fish bladder system for robot fish. *2011 IEEE International Conference on Robotics and Biomimetics*, 2126–2130. https://doi.org/10.1109/ROBIO.2011.6181606

Morawski, M., Malec, M., Szymak, P., & Trzmiel, A. (2014). Analysis of parameters of traveling wave impact on the speed of biomimetic underwater vehicle. In *Solid State Phenomena* (Vol. 210). https://doi.org/10.4028/www.scientific.net/SSP.210.273

Morawski, M., Słota, A., Zając, J., & Malec, M. (2020). Fish-like shaped robot for underwater surveillance and reconnaissance – Hull design and study of drag and noise. *Ocean Engineering*, *217*(March), 1–10. https://doi.org/10.1016/j.oceaneng.2020.107889

Morawski, M., Słota, A., Zając, J., Malec, M., & Krupa, K. (2018). Hardware and low-level control of biomimetic underwater vehicle designed to perform ISR tasks. *Journal of Marine Engineering and Technology*, *16*(4). https://doi.org/10.1080/20464177.2017.1387089

Morgansen, K.A., Triplett, B.I., & Klein, D.J. (2007). Geometric Methods for Modeling and Control of Free-Swimming Fin-Actuated Underwater

Vehicles. *IEEE Transactions on Robotics*, *23*(6), 1184–1199. https://doi.org/10.1109/LED.2007.911625

Nguyen, Q.S., Park, H.C., & Byun, D. (2011). Thrust Analysis of a Fish Robot Actuated by Piezoceramic Composite Actuators. *Journal of Bionic Engineering*, *8*(2), 158–164. https://doi.org/10.1016/S1672-6529(11)60019-X

Nguyen, T.-T., Nguyen, N.-P., & Dang, M.-N. (2011). Swimming of robotic fish based biologically-inspired approach. *11th International Conference on Control*, *Automation and Systems (ICCAS)*, 625–630. http://ieeexplore.ieee.org/xpls/abs_all.jsp?arnumber=6106079

Niu, C., Zhang, L., Bi, S., & Cai, Y. (2012). Development and depth control of a robotic fish mimicking cownose ray. *Proceedings of the 2012 IEEE International Conference on Robotics and Biomimetics*, *ROBIO 2012*, 814–818. https://doi.org/10.1109/ROBIO.2012.6491068

Robert, K., Huvenne, V.A.I., Georgiopoulou, A., Jones, D.O.B., Marsh, L.D.O., Carter, G., & Chaumillon, L. (2017). New approaches to high-resolution mapping of marine vertical structures. *Scientific Reports*, *7*(1), 9005. https://doi.org/10.1038/s41598-017-09382-z

Singh, W., Örnólfsdóttir, E.B., & Stefansson, G. (2014). A Small-Scale Comparison of Iceland Scallop Size Distributions Obtained from a Camera Based Autonomous Underwater Vehicle and Dredge Survey. *PLoS ONE*, *9*(10), e109369. https://doi.org/10.1371/journal.pone.0109369

Tangorra, J.L., Mignano, A.P., Carryon, G.N., & Kahn, J.C. (2011). Biologically derived models of the sunfish for experimental investigations of multi-fin swimming. *2011 IEEE/RSJ International Conference on Intelligent Robots and Systems*, 580–587. https://doi.org/10.1109/IROS.2011.6095094

Wen, L., Wang, T., Wu, G., Liang, J., & Wang, C. (2012). Novel Method for the Modeling and Control Investigation of Efficient Swimming for Robotic Fish. *IEEE Transactions on Industrial Electronics*, *59*(8), 3176–3188. https://doi.org/10.1109/TIE.2011.2151812

Xiang, X., Yu, C., Niu, Z., & Zhang, Q. (2016). Subsea cable tracking by autonomous underwater vehicle with magnetic sensing guidance. *Sensors (Switzerland)*, *16*(8), 1–22. https://doi.org/10.3390/s16081335

Yao, X., Yang, G., & Peng, Y. (2017). Nonlinear Reduced-Order Observer-Based Predictive Control for Diving of an Autonomous Underwater Vehicle. *Discrete Dynamics in Nature and Society*, *2017*, 1–15. https://doi.org/10.1155/2017/4394571

Yu, J., Sun, F., Xu, D., & Tan, M. (2016). Embedded Vision-Guided 3-D Tracking Control for Robotic Fish. *IEEE Transactions on Industrial Electronics*, *63*(1), 355–363. https://doi.org/10.1109/TIE.2015.2466555